Review in Advance first posted online on October 17, 2011. (Changes may still occur before final publication online and in print.)

# Physics and Computation of Aero-Optics

Meng Wang,[1] Ali Mani,[2] and Stanislav Gordeyev[1]

[1]Department of Aerospace and Mechanical Engineering, University of Notre Dame, Notre Dame, Indiana 46556; email: m.wang@nd.edu, sgordeye@nd.edu

[2]Department of Chemical Engineering, Massachusetts Institute of Technology, Cambridge, Massachusetts 02139; email: alimani@mit.edu



Annu. Rev. Fluid Mech. 2012. 44:299–321

The *Annual Review of Fluid Mechanics* is online at fluid.annualreviews.org

This article's doi: 10.1146/annurev-fluid-120710-101152



0066-4189/12/0115-0299$20.00

## Keywords

wave-front distortion, turbulent flow, high-fidelity simulation, optical mitigation

## Abstract

This article provides a critical review of aero-optics with an emphasis on recent developments in computational predictions and the physical mechanisms of flow-induced optical distortions. Following a brief introduction of the fundamental theory and key concepts, computational techniques for aberrating flow fields and optical propagation are discussed along with a brief survey of wave-front sensors used in experimental measurements. New physical understanding generated through numerical and experimental investigations is highlighted for a number of important aero-optical flows, including turbulent boundary layers, separated shear layers, and flow over optical turrets. Approaches for mitigating aero-optical effects are briefly discussed.

## 1. INTRODUCTION

Distortions of optical signals by turbulent flow are widely observed in nature and in technological applications. The twinkling of stars, or stellar scintillation, is the result of the refraction of light (electromagnetic waves) by turbulent fluctuations in Earth's atmosphere. Shadowgraphs and schlieren are popular flow visualization techniques that exploit optical distortions to visualize the flow field that produced them. Over the past four decades, much attention has been paid to the aero-optical effects on the performance of airborne laser systems for communication, target tracking, and directed-energy weapons. In these systems, optical distortions produced by turbulent flows surrounding the projection aperture pose a serious problem, causing beam distortion, jitter, and much reduced effective range. The performance of airborne and ground-based imaging systems is similarly impaired by turbulent flows in the vicinity of the viewing aperture.

The direct cause of optical distortions is density variations in the flow field. For air and many other fluids, the index of refraction is linearly related to the density of the fluid by the Gladstone-Dale relation (Wolfe & Zizzis 1978). When a beam of an initially planar wave front is transmitted through a variable density field, different parts of the beam propagate at different local speeds of light, resulting in distortions of the wave front, as shown schematically in **Figure 1**. An optical beam emitted from a projection aperture, or received by a viewing aperture, typically transmits/receives through two distinct flow regions: (*a*) the active turbulence region induced by solid objects near the optical window and (*b*) atmospheric turbulence. The propagation through atmospheric turbulence has been studied extensively (Chernov 1960, Tatarski 1961) and is relatively well understood. Because of the large temporal and spatial scales associated with atmospheric turbulence, its aberrating effects are of low frequency (<100 Hz) and can be largely corrected using adaptive-optics systems (e.g., Hardy 1998, Lloyd-Hart 2003). In contrast, the turbulent flow induced by solid surfaces near the aperture, which may comprise turbulent boundary layers, free-shear layers, wakes, and shock waves for supersonic and transonic flows, is characterized by much smaller turbulence scales. The size of the optically active flow region is typically thinner than or comparable with the aperture size. Aero-optics, to follow the conventional definition (Gilbert & Otten 1982, Sutton 1985, Jumper & Fitzgerald 2001), is concerned with the aberrating effects of compressible

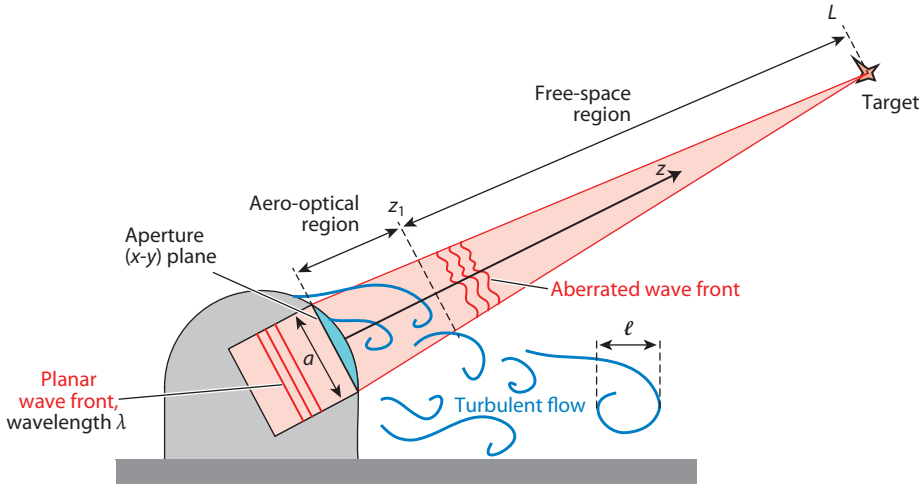


**Figure 1**

Schematic of the aero-optics problem.

turbulence in this region. Compared to the atmospheric boundary layer, the aero-optical flow generates stronger optical aberrations at smaller scales and higher frequencies, which are beyond the capability of today's adaptive-optics technology. Mitigation of these aberrations via active and passive flow control has been actively pursued in recent years (e.g., Gordeyev et al. 2010a,b).

The types of aero-optical distortions and their far-field impact depend on a number of physical and geometric parameters, including the optical wavelength $\lambda$, the aperture or beam size $a$, the turbulence length scale $\ell$ of the aberrating field, and the distance of propagation $L$ (see **Figure 1**). In crude terms, small-scale turbulence, with eddy sizes less than the optical aperture ($\ell < a$), causes optical scattering, beam spread, and consequent attenuation of intensity, whereas turbulent eddies larger than or comparable in size to the aperture ($\ell \geq a$) are mostly responsible for the unsteady tilt of the beam or beam jitter (Cassady et al. 1989). In addition, the mean density gradient in the beam path causes steady wave-front distortions known as the lensing effect. The magnitude of wave-front distortions $\mathrm{OPD}_{rms}$ (its precise definition is given below) is generally small in an absolute sense but can be a significant fraction of, or even exceed, the optical wavelength. In other words, the optical phase distortion $2\pi\,\mathrm{OPD}_{rms}/\lambda$, which determines the far-field beam quality, can be easily of $O(0.1)$ to $O(1)$. For the same distortion magnitude, the phase distortion of an aberrated beam is inversely proportional to the optical wavelength, making the aero-optics problem particularly acute for short-wavelength beams (Jumper & Fitzgerald 2001). This poses a significant impediment to the use of shorter-wavelength laser systems, which are preferred in the absence of aero-optical aberrations; for an unaberrated beam with fixed output power, the diffraction-limited optical intensity scales with $a^2/(L^2\lambda^2)$ (Born & Wolf 2002).

A number of review articles have been written on aero-optics. Research in the pre-1980 era has been documented by Gilbert & Otten (1982). Progress since then has been surveyed by Sutton (1985), Jumper & Fitzgerald (2001), and more recently Gordeyev & Jumper (2010) with a focus on the aero-optics of turrets. Among recent advances in this field are high-speed and high-resolution wave-front sensors that allow measurements of instantaneous wave-front errors in unprecedented detail and the increasing role played by numerical simulations. The application of computational fluid dynamics (CFD) to aero-optics problems has historically lagged behind most other areas because of the challenging nature of the computations, which must be time accurate and compressible and capture optically important flow scales. However, this has begun to change with recent advances in high-fidelity simulation tools and the concomitant increase in computing power. A new generation of computational techniques, including direct numerical simulation (DNS), large-eddy simulation (LES), and hybrid methods combining LES with Reynolds-averaged Navier-Stokes (RANS) approaches, has been employed hand in hand with experimental and theoretical approaches to elucidate the physics of aero-optics, predict aberration effects, and develop techniques for their mitigation. This article attempts to provide a critical review of some recent progress in the understanding and prediction of aero-optical effects. The discussion is primarily from a computational perspective, although important experimental findings are also included.

## 2. THEORETICAL BACKGROUND

### 2.1. Basic Equations

The theoretical foundation for electromagnetic wave propagation in a turbulent medium is discussed extensively by Monin & Yaglom (1975, chapter 9) and is briefly outlined here in the context of aero-optics. In the most general sense, the propagation of electromagnetic waves is governed by the Maxwell equations along with compressible Navier-Stokes equations. Various simplifications can be made depending on relevant physical parameters, length scales, and timescales. For aero-optical problems, the timescale for optical propagation is negligibly short relative to flow

timescales, and hence optical propagation can be solved in a frozen flow field at each time instant. If the optical wavelength is much shorter than the smallest flow scale (Kolmogorov scale), which is generally the case, the effect of depolarization is negligible, and the Maxwell equations reduce to a vector wave equation in which all three components of the electromagnetic field are decoupled. A scalar component of the electric field at frequency $\omega$ is governed by

$$\nabla^2 U + \frac{\omega^2 n^2}{c_0^2} U = 0, \tag{1}$$

where $c_0$ is the speed of light in vacuum, and $n$ is the index of refraction. The latter is related to the density of air via the Gladstone-Dale relation: $n(x, y, z) = 1 + K_{GD}(\lambda)\rho(x, y, z)$, where $K_{GD}$ is the Gladstone-Dale constant and is in general weakly dependent on the optical wavelength (Wolfe & Zizzis 1978). In aero-optics, fluctuations in the index of refraction are small ($\sim 10^{-4}$) and have scales much larger than the optical wavelength; hence an optical beam propagates predominantly in the axial ($z$) direction with slowly varying amplitude. It is customary to invoke the paraxial approximation, which assumes $U(x, y, z) = A(x, y, z)\exp(-ikz)$ and $|\partial^2 A/\partial z^2| \ll |k\partial A/\partial z|$, where $k = \omega/c_\infty$ is the optical wave number in the free stream. This leads to the parabolized wave equation for the complex amplitude

$$-2ik\frac{\partial A}{\partial z} + \nabla_\perp^2 A + k^2\left(\frac{n^2}{n_\infty^2} - 1\right)A = 0, \tag{2}$$

where $\nabla_\perp^2$ is the Laplacian operator in the transverse directions. Not included in the paraxial wave equation are large-angle scattering and energy dissipation/absorption, which are insignificant for aero-optical problems. Monin & Yaglom (1975, chapter 9) discuss in detail the approximations leading to the paraxial wave equation and its limitations of applicability.

Further approximations can be made to obtain closed-form solutions to Equation 2. As depicted schematically in **Figure 1**, the propagation domain consists of two distinct regions: the optically active turbulent near field (from $z = 0$ to $z_1$) and the free space extending to the distant far field (from $z = z_1$ to $L$, with $L \gg z_1$). For transmission across the aero-optical region, it can be shown that the contribution from the Laplacian term in Equation 2, which represents the diffraction effect, is negligible relative to the last term for $z_1 \ll \ell_\perp^2/\lambda$, where $\ell_\perp$ is the transverse length scale of the optical wave. If the refractive index is expressed as $n = n_\infty + n'$, and the linear approximation $n^2/n_\infty^2 \approx 1 + 2n'/n_\infty$ is made about the index-of-refraction deviation from the free-stream value, Equation 2 can be integrated from 0 to $z_1$ to obtain $A(x, y, z_1) = A(x, y, 0)\exp[-\frac{ik}{n_\infty}\int_0^{z_1} n'(x, y, z)dz]$, or

$$U(x, y, z_1) = U(x, y, 0)\exp\left[-ik_0\int_0^{z_1} n(x, y, z)dz\right], \tag{3}$$

where $k_0 = k/n_\infty = \omega/c_0 = 2\pi/\lambda_0$ is the optical wave number in vacuum.

Once the solution past the aero-optical region, $U(x, y, z_1)$, has been determined, it can be used as the initial condition to propagate the optical beam to the far field using the wave equation (Equation 1) or paraxial wave equation (Equation 2). By setting $n = n_\infty$ and $n' = 0$, either equation can be solved analytically using Fourier transform techniques, which are the basis for Fourier optics (Goodman 2004).

## 2.2. Near-Field Distortion Measures

Equation 3 suggests that the dominant aero-optical effect after transmission through the turbulence region is a phase distortion of the optical wave front; the amplitude is approximately

unchanged. The integral in Equation 3 is known as the optical path length (OPL). It is most commonly derived from geometric optics by assuming straight ray paths and is generally dependent on the flow timescale (but not the optical timescale):

$$\mathrm{OPL}(x, y, t) = \int_0^{z_1} n(x, y, z, t) dz. \tag{4}$$

Ray bending can be accounted for by solving the eikonal equation (Born & Wolf 2002) but is generally negligible for aero-optics. In practice, the relative difference in the OPL over the aperture is a more relevant representation of wave-front distortions. It is called the optical path difference (OPD) and is defined as

$$\mathrm{OPD}(x, y, t) = \mathrm{OPL}(x, y, t) - \langle \mathrm{OPL}(x, y, t) \rangle, \tag{5}$$

where the angle brackets denote spatial averaging over the aperture. The optical phase distortion is then $2\pi \mathrm{OPD}/\lambda$. We note that the optical wave front, defined as the locus of constant phase, is (after removing the spatial mean) the conjugate (negative) of the OPD: $W(x, y, t) = -\mathrm{OPD}(x, y, t)$.

To facilitate analysis and mitigation of distortions, researchers often decompose the time-dependent OPD into a time-averaged spatial component, called the steady-lensing term, $\mathrm{OPD}_{\mathrm{steady}}(x, y)$, and an unsteady component. The unsteady part can be further split into a spatially linear component, called unsteady tilt or beam jitter, and the rest, usually called high-order distortions (Gordeyev & Jumper 2010). In other words,

$$\mathrm{OPD}(x, y, t) = \mathrm{OPD}_{\mathrm{steady}}(x, y) + [A(t)x + B(t)y] + \mathrm{OPD}_{\mathrm{high\text{-}order}}(x, y, t). \tag{6}$$

Physically, these three components affect an outgoing beam in different ways. The steady-lensing term, $\mathrm{OPD}_{\mathrm{steady}}(x, y)$, is a function only of the time-averaged density field and imposes a steady distortion such as a defocus or coma. The tilt or jitter, represented by the second term on the right-hand side, does not change the spatial distribution of the outgoing beam but simply redirects it in directions defined by functions $A(t)$ and $B(t)$. The specific forms of $A(t)$ and $B(t)$ depend on the definition of tilt. For the so-called $G$ tilt (Tyson 2000), $A(t)$ and $B(t)$ are the spatially averaged gradient components of the OPD in the $x$ and $y$ directions, respectively, whereas for the $Z$ tilt (Sasiela 2007), they are defined such that the magnitude of $\mathrm{OPD}_{\mathrm{high\text{-}order}}$ in Equation 6 is minimized in the least-squares sense at each time instant. Finally, the high-order term causes the beam to change its shape and intensity distribution.

The decomposition in Equation 6 is particularly useful when an adaptive optics system is used to correct for aberrating wave fronts. The purpose of an adaptive optics system is to apply a conjugate wave front to the outgoing beam so that it will negate optical aberrations from the flow, and the beam will become recollimated after passing through the turbulent media (Tyson 1997). Among the distortion components given in Equation 6, steady lensing is easily corrected by a deformable mirror with a large range of motion, the tilt component is removed using a fast-steering mirror, and the high-order term can be compensated for by using a high-bandwidth deformable mirror (Tyson 1997).

## 2.3. Statistical Theory

An important equation relating the statistical properties of a turbulent medium and those of aero-optical aberrations, the so-called linking equation, was first derived by Sutton (1969). In the most general form, the linking equation can be written as (Steinmetz 1982, Havener 1992)

$$\overline{\langle \mathrm{OPD}^2 \rangle} = K_{GD}^2 \int_0^{z_1} \int_0^{z_1} \mathrm{Cov}_{\rho'}(z, z') \mathrm{d}z' \mathrm{d}z, \tag{7}$$

where the overbar denotes time averaging, $\mathrm{Cov}_{\rho'}$ is the covariance function of density fluctuations, and $z_1$ is the integration distance along the traversing beam through the turbulence region. In the case of homogeneous turbulent flows, the density covariance is most commonly modeled by an exponential function (Steinmetz 1982), $\rho_{rms}^2 \exp(-|z - z'|/\Lambda)$, or a Gaussian function (Wolters 1973), $\rho_{rms}^2 \exp(-|z - z'|^2/\Lambda^2)$, where $\Lambda$ is the characteristic length scale for density fluctuations. Substituting these models into Equation 7 leads to

$$\overline{\langle \mathrm{OPD}^2 \rangle} = \alpha K_{GD}^2 \int_0^{z_1} \rho_{rms}^2(z)\Lambda(z)\mathrm{d}z, \tag{8}$$

where $\alpha = 2$ for the exponential covariance function and $\sqrt{\pi}$ for the Gaussian covariance function. Both the density fluctuation magnitude and length scale are allowed to vary slowly along the beam path. With $\alpha = 2$, Equation 8 is the original form of Sutton's linking equation (Sutton 1969).

Both forms of the linking equation allow one to calculate aero-optical distortions indirectly from statistical properties of the turbulent flow. Because the full covariance matrix in Equation 7 is difficult to measure experimentally, the simplified equation (Equation 8) is commonly used instead. However, as the simplified linking equation is derived for locally homogeneous turbulence in the direction of propagation, its applicability to inhomogeneous flows, such as shear layers (Hugo & Jumper 2000) and boundary layers (Gilbert & Otten 1982, Tromeur et al. 2006a), has been questioned. It has been shown that with appropriate choice of the length scale $\Lambda_\rho$, the simplified linking equation can be used to obtain accurate results for inhomogeneous turbulent flow fields. The key is to use the correct density correlation length defined based on Equation 7 (Wang & Wang 2011).

## 3. PREDICTION OF FAR-FIELD DISTORTIONS

Given the OPD profiles after the beam passes the turbulence region, one can solve its free-space propagation from $z = z_1$ to $L$ using Fourier optics to obtain the exact far-field projection. **Figure 2** shows an example of the instantaneous far-field irradiance of a Gaussian beam subject to strong aero-optical distortions by the turbulent wake behind a circular cylinder of diameter $D$ (Mani et al. 2009). It contrasts the distorted beam pattern with that of an undistorted, diffraction-limited beam for two different optical wavelengths. In this case, the near-field $\mathrm{OPD}_{rms}$ is $6.7 \times 10^{-6} D$, corresponding to phase distortions of $2\pi\mathrm{OPD}_{rms}/\lambda \approx 17$ and 4.2 for the two wavelengths (6.7 and 1.7, respectively, after tilt removal). Drastic losses of far-field beam intensity and coherence are observed. In the absence of distortions, the shorter-wavelength beam delivers more energy to the target than the longer-wavelength one, but this advantage is offset by aero-optical distortions. In fact, the ratio of the maximum intensity of the distorted beam to that of the undistorted one is approximately 1.5% for the shorter-wavelength case and 10% for the longer-wavelength case.

Although Fourier optics provides a complete description of the optical propagation, it requires as input a detailed spatiotemporal history of the near-field wave front, which may not be readily available. Furthermore, from a systems point of view, statistical measures, rather than instantaneous quantities, are of primary interest, and it is desirable to relate the far-field beam statistics to statistics of the aberrating flow field. A widely adopted relation is the Maréchal approximation (Maréchal 1947, Born & Wolf 2002) for the Strehl ratio (SR), defined as the ratio of the peak on-axis far-field irradiance of an aberrated beam (after tilt removal) to the corresponding peak irradiance of an unaberrated beam; it is a measure of beam quality relative to a diffraction-limited beam at each time instant. In his original paper, Maréchal (1947) showed that, in the limit of small phase distortions, $\mathrm{OPD}_{rms}/\lambda < 0.1$, $\mathrm{SR}(t) = I(t)/I_0 \approx 1 - [2\pi\mathrm{OPD}_{rms}(t)/\lambda]^2$. A more commonly

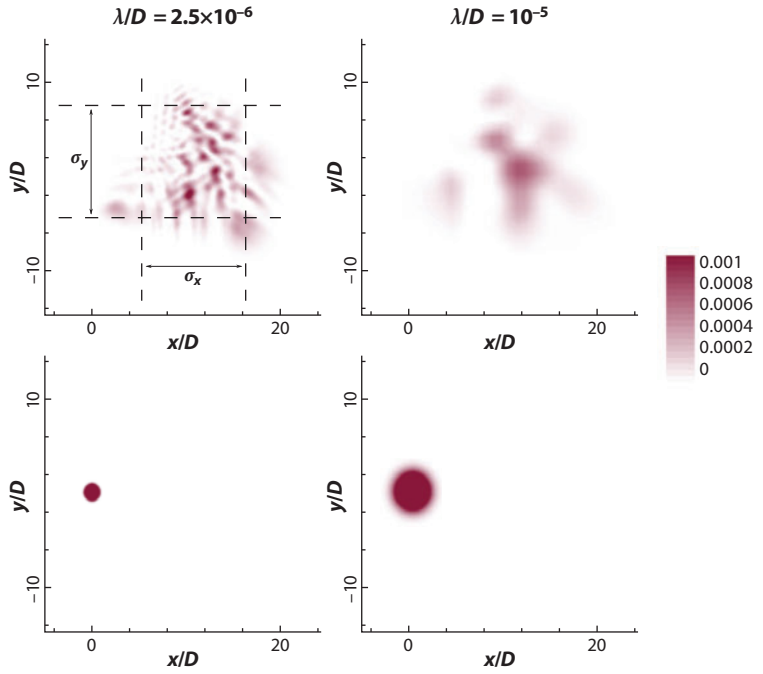


**Figure 2**

Instantaneous far-field optical irradiance for Gaussian beams through the wake of a circular cylinder of diameter $D$ at a distance of $10^5 D$ for two optical wavelengths. The top plots show the distorted beams, and the bottom plots show the undistorted, diffraction-limited beams. The aperture diameter is $a = 0.3D$. The peak dimensionless intensities (relative to the aperture value) for the undistorted beams are 0.074 and 0.005 for $\lambda/D = 2.5 \times 10^{-6}$ and $10^{-5}$, respectively. The results are obtained using large-eddy simulations at a free-stream Mach number $M = 0.4$ and Reynolds number $Re_D = 3{,}900$ (Mani et al. 2009).

adopted expression, however, takes the exponential form

$$\frac{I(t)}{I_0} = \mathrm{SR}(t) \approx \exp\left\{-\left[\frac{2\pi \mathrm{OPD}_{rms}(t)}{\lambda}\right]^2\right\}. \tag{9}$$

This equation, also known as the Maréchal approximation, was proposed by Mahajan (1982, 1983) based on empirical fitting of the SR versus $\mathrm{OPD}_{rms}$ data for a variety of distortion modes. In comparison with the original form, Mahajan found that Equation 9 gave a better approximation for the SR over a wider range of phase distortions.

Ross (2009) recently re-examined the derivation of the Maréchal approximation and found that for OPD data with a Gaussian probability density distribution, Equation 9 was in fact exact. It is important to note that the original Maréchal approximation is a relationship between the spatial statistics of the instantaneous wave front and the far-field intensity. In the case in which the aperture size is much larger than the turbulence length scale, $a \gg \ell$, Steinmetz (1982) showed that the Maréchal approximation is also approximately valid for the time-averaged SR:

$$\overline{\mathrm{SR}} \approx \exp\left[-\overline{\left(\frac{2\pi \mathrm{OPD}_{rms}}{\lambda}\right)^2}\right]. \tag{10}$$

This equation is known interchangeably as the large-aperture approximation and Maréchal approximation. However, in many practical applications, the assumptions of large (infinite) aperture and small aberrations are not exactly valid. For stationary, Gaussian-in-space processes, an exact version of the time-averaged Maréchal approximation can be expressed in terms of the temporal probability density function of $\mathrm{OPD}_{rms}$ (Porter et al. 2011).

The time-averaged version of the Maréchal approximation is currently the de facto standard approach for estimating and comparing the effect of aero-optical distortions on the degradation of beam performance. Despite its routine use, some uncertainties still exist concerning the accuracy and applicability of this approximation, particularly for cases with large phase distortions.

Mani et al. (2006) proposed a new set of statistical measures to quantify the far-field optical distortions and derived exact algebraic relations between these measures and the statistics of the near-field OPD. Instead of characterizing beam distortions in terms of peak irradiance, they proposed the use of the spatial spread of the beam, in terms of the second spatial moment of the far-field irradiance, as a measure of distortion (see **Figure 2**). Through statistical solutions of the paraxial wave equation, they showed that the square of the beam spread about its center (i.e., with tilt removal) can be expressed, in the Fraunhofer limit $L\lambda/a^2 \gg 1$, as

$$\left(\frac{\sigma_x}{L}\right)^2 = C\frac{\lambda^2}{\pi^2 a^2} + \left\langle \left(\frac{\partial}{\partial x}\mathrm{OPD}\right)'^2 \right\rangle, \tag{11}$$

where $\sigma_x$ is the beam spread in the $x$ direction, $a$ is the aperture diameter, the prime represents deviation from the mean value, and the angle brackets indicate a spatial average. $C$ is a constant determined by the shape of the aperture and its optical intensity profile; it is an $O(1)$ quantity for beams with smooth aperture intensity profiles and is exactly equal to 1 for Gaussian beams. The beam spread in the $y$ direction (see **Figure 2**) has the same form. One can observe clearly that the anisotropy of the beam spread about its axis is directly linked to the anisotropy of OPD gradients and thus in the refractive-index field.

The first term on the right-hand side of Equation 11 represents the effect of diffraction on the beam spread, which is decoupled from the aero-optical effect represented by the second term. The latter is simply the variance of the OPD gradient. The ratio of these two terms was proposed by Mani et al. (2006) as the basis for a new distortion measure, which they termed the fidelity ratio. Compared with the SR based on the Maréchal approximation, the new measure has the advantage of being applicable to highly aberrated beams because Equation 11 is exact. Also, it gives an estimate of the sensor size needed to record the signal. Whereas a disadvantage is that its applicability is limited to beams with initially smooth (continuous) aperture intensity profiles as the beam spread becomes singular for beams with discontinuous intensity profiles, the use of the information gained by assuming a continuous intensity profile provides valid insight into how even a discontinuous intensity beam will perform. Equation 11 also provides insight into the scaling of aero-optical distortions with key optical parameters such as the aperture size. For instance, one can expect that the aero-optical effect is a lesser concern for the naked human eye (with $a \sim 1$ mm) compared to a tactical airborne system (with $a \sim 20$ cm) because the far-field resolution of the human eye is predominantly limited by the diffraction term for typical aero-optical flows.

## 4. COMPUTATIONAL AND EXPERIMENTAL APPROACHES

### 4.1. Computational Methods

Computations of aero-optics consist of two essential parts: solutions of the aberrating flow field via CFD techniques and propagation of the optical beam through the aberrating flow to the

target. Solution methods for both are discussed below, with and emphasis on the computation of aberrating flows.

**4.1.1. Optical propagation.** In practice, the beam propagation is easily computed by a combination of ray tracing with Fourier optics. For propagation through the thin aero-optical region surrounding an aperture, ray optics is applicable, and Equation 3 or its OPD representation provides satisfactory results. The numerical evaluation involves a simple integration of the index-of-refraction field along the optical path. The validity of this approach has been established based on scaling arguments and has been confirmed numerically by White (2010) through a comparison with the numerical solution of the paraxial wave equation (Equation 2) using a high-order scheme in the case of optical propagation through a supersonic turbulent boundary layer. Beyond the aero-optical region, the index of refraction is considered uniform, and propagation in free space can be treated with Fourier optics, as exemplified in Section 3. If the target is in the optical far field, the Fraunhofer approximation (Goodman 2004) can be applied to simplify the solution.

The long-range propagation of optical waves in atmospheric turbulence is significantly more difficult to compute. Ray tracing is invalid because amplitude variations accumulated over a large distance are significant, and numerical solutions of the wave equation or paraxial wave equation are impeded by the vast scale disparity and prohibitive computational expenses required to obtain the fluctuating index-of-refraction field over the entire propagation range. Current approaches are predominantly based on statistical modeling of the turbulent media in terms of discrete thin phase screens along the direction of propagation and numerical integration of the paraxial wave equation (e.g., Coles et al. 1995, Frehlich 2000). Because its distortion effect can be corrected by adaptive-optics techniques, atmospheric propagation is not considered a pressing issue in aero-optics and is therefore not discussed further.

**4.1.2. Computation of aberrating flows.** The most challenging part of computational aero-optics is the computation of the aberrating flows surrounding optical apertures. These flows are compressible, turbulent, and generally three dimensional at high Reynolds numbers, often with separation. To accurately compute the index-of-refraction field, one must capture turbulence scales over all optically relevant wave numbers and frequencies, which poses a significant challenge in terms of computational expenses and numerical accuracy. Because of these difficulties, the application of CFD to aero-optics did not start until the late 1980s, and significant growth occurred only in the past decade as a result of the advancement and maturation of high-fidelity simulation techniques.

Limited by computing power, early numerical investigations involved two-dimensional solutions of Euler and RANS equations. Cassady et al. (1989) performed RANS simulations of the flow over an open cavity in the Mach number range between 0.6 and 0.8 under standard conditions at altitudes of 40,000 to 50,000 ft and analyzed image distortions at different look angles across the shear layer. Because their RANS calculations did not capture the coherent structures in the shear layer, only the steady tilt of the optical beam was predicted directly. Beam jitter was modeled, and high-order distortions were largely unaccounted for. Tsai & Christiansen (1990) solved Euler equations numerically to study the degradation of a laser beam by a plane mixing layer at low Mach numbers ($M_1 = 0.2$ and $M_2 = 0.1$ for the two air streams). Their solutions were able to capture qualitative features of large-scale coherent structures including vortex pairing, but this is a result of the numerical viscosity in the simulation code based on a combination of MacCormack and Godunov methods.

Although the Euler and RANS solutions are computationally efficient, their usefulness for aero-optical predictions is limited. Euler equations do not describe the correct physics of

refractive-index fluctuations in a turbulent flow and must rely on numerical dissipation to mimic the effect of physical viscosity. In a steady RANS calculation, all turbulence scales are modeled, resulting in an ensemble-averaged (time-averaged) density field from which the steady-lensing effect of optical aberrations can be evaluated but not the unsteady tilt and high-order effects. It is, however, possible to combine a RANS simulation with a statistical model for optics, such as the linking equation (Equation 8), to estimate the aero-optical effects. This provides a practical approach for high-Reynolds-number flows in realistic configurations that is not currently affordable with more accurate techniques. Smith et al. (1990) proposed a transport equation for the variance of index-of-refraction fluctuations and solved it along with compressible turbulent boundary-layer equations with a $k - \varepsilon$ model for a plane mixing layer. The computed refractive-index variance, together with the turbulence length scale estimated based on $k$ and $\varepsilon$ solutions, allowed the linking equation to predict the wave-front error for a beam passing the mixing layer and its impact on target intensity. Using the same methodology, Pond & Sutton (2006) performed an aero-optic analysis of a nose-mounted optical turret on an aircraft. Their solutions are based on three-dimensional RANS equations, the $k - \varepsilon$ model, and the transport equation for the refractive-index variance proposed by Smith et al. (1990).

For more accurate computations of index-of-refraction fluctuations, a hierarchy of high-fidelity methods, including DNS, LES, and hybrid RANS/LES approaches, is available. Among them, DNS (Moin & Mahesh 1998), which resolves all flow scales down to the dissipative scale, is the most accurate. Because of the well-known Reynolds-number limitation, it is primarily a research tool and has found only limited use in aero-optics. Truman & Lee (1990) and Truman (1992) used DNS data to investigate the phase distortions in optical beams through a homogeneous shear flow with uniform mean shear and a turbulent channel flow. Their simulations were based on incompressible Navier-Stokes equations, and the fluctuating index-of-refraction field was represented as a passive scalar. They found that the magnitude of the phase distortions was sensitive to the direction of propagation, which they explained in terms of the anisotropic vortical structures in the flow. Despite the low Reynolds numbers and incompressible nature of the simulations, the findings in these studies are qualitatively consistent with subsequent experimental measurements (Cress et al. 2008) and results of compressible flow simulations (Wang & Wang 2009) (see Section 5.1).

LES offers a less expensive alternative to DNS because it resolves only the large, energy-containing scales of fluid motions that are optically important. The effects of small scales are modeled by a subgrid-scale (SGS) model. The prevalent SGS models in use today are of the Smagorinsky eddy-viscosity type (Smagorinsky 1963) for which the dynamic procedure (Germano et al. 1991, Moin et al. 1991, Lilly 1992) provides a robust way of computing the model coefficient from the resolved scales, thus eliminating the need for adjustable model parameters. Some practitioners use implicit LES (ILES) in which a high-order low-pass spatial filter acts as the SGS model to selectively provide numerical dissipation (e.g., Visbal 2009, White et al. 2010), often out of numerical-stability consideration for high-order accurate compressible LES codes.

The first application of LES to aero-optics was made by Childs (1993), who carried out the LES of high-speed turbulent mixing layers at convective Mach numbers of up to 2.5 and analyzed the induced wave-front distortions. Significant growth in LES-based investigations occurred in the past decade as a result of the maturation of LES methodology, advances in computing power, and a renewed interest in the field of aero-optics. LES has been employed in a variety of aero-optical configurations, including turbulent shear layers (Visbal 2008, 2009; White et al. 2010), open-cavity flows (Sinha et al. 2004, Visbal 2008), turbulent boundary layers (Tromeur et al. 2003, 2006a,b; Wang & Wang 2009, 2011; White & Visbal 2010), flow over a cylinder (Mani et al. 2009), and flows over cylindrical turrets (Wang & Wang 2009, Morgan & Visbal 2010, Wang et al. 2010) and realistic three-dimensional turrets (Jones & Bender 2001, Arunajatesan &

Sinha 2005). In addition, there have been attempts to employ LES to predict the effect of passive flow control on aero-optical mitigation (Morgan & Visbal 2010, Wang et al. 2010). Among the above-mentioned studies, simple canonical flows such as turbulent shear layers, boundary layers, and flow over a cylinder were simulated to study the fundamental physics of aero-optics and were afforded adequate grid resolution and numerical accuracy. We discuss some of these findings in Section 5. Conversely, the simulations of three-dimensional turret flows were under-resolved and used simulation codes with large numerical dissipation.

To further reduce computational costs for wall-bounded flows at high Reynolds numbers, one can combine LES with a RANS model to form a hybrid RANS/LES method. A popular class of hybrid methods, proposed and recently reviewed by Spalart (2009), is detached-eddy simulation (DES). In this method, less expensive RANS equations are solved with an appropriate turbulence model in an attached boundary layer, and LES is used to treat the separated-flow region. It therefore avoids the stringent boundary-layer resolution demanded for LES but at the same time inherits many weaknesses of RANS methods, such as the poor prediction of pressure-driven incipient separation. In addition, the lack of turbulent fluctuations prior to separation may affect the instability of the separated shear layer and its aero-optical behavior. The presence of turbulent fluctuations is particularly important for evaluating some passive flow–central approaches that depend on introducing small-scale disturbances into the boundary layer prior to separation. DES and similar hybrid methods have been applied in simulations of flow over three-dimensional optical turrets, with limited success (Nahrstedt et al. 2008, Ladd et al. 2009, Morgan & Visbal 2010) (for more discussion, see Section 5.3). Another class of hybrid methods, which is more accurate and robust but computationally more demanding than DES, is LES with wall modeling (Piomelli & Balaras 2002, Wang & Moin 2002). In this case, only the near-wall region in a turbulent boundary layer is treated with RANS modeling, whereas the bulk part of the boundary layer is computed using LES. This avoids the strong Reynolds-number scaling of grid-resolution requirements in a fully resolved LES. LES with wall modeling has not been used for aero-optical computations but holds promise as computing power continues to grow.

### 4.2. Resolution Requirements

Turbulent flows relevant to aero-optics contain eddies over a wide range of scales, typically from the order of meters to the order of 10 μm. When practical computational tools such as LES are employed for aero-optical computations, it is important to ensure that the optical effects of the unresolved flow are negligible. Addressing this issue requires an understanding of the range of optically active flow scales in aero-optical flows. Such knowledge not only helps select the mesh size for computations, but also provides insight for adaptive-optics requirements. In other words, if the distortion effects are to be canceled by deformable mirrors, the range of length scales (and frequencies) to be corrected can be determined from the same theory.

From Equation 3, it is clear that a lack of flow resolution will cause errors in the computation of the optical phase when the beam is traced through the turbulence. If the true refractive-index field is written in terms of the resolved field, $n_r$, and the error, $n_e$, which is basically the unresolved $n$, substituting $n = n_r + n_e$ into Equation 3 yields

$$U(x, y, z_1) \simeq U_r(x, y, z_1) - \left[ ik_0 \int_0^{z_1} n_e(x, y, z) dz \right] U_r(x, y, z_1), \tag{12}$$

where a leading-order expansion for small $n_e$ is used, and $U_r$ is the computed optical wave (by substituting the resolved field, $n_r$, into Equation 3). According to this description, the true optical wave at $z_1$ is written in terms of two beams: The first term on the right-hand side represents the

computed beam, and the second term represents the "error beam" associated with the lack of resolution in predicting the refractive-index field. An acceptable resolution should ensure that the energy of the error beam is much smaller than the energy of the resolved beam.

Mani et al. (2008) used this criterion in conjunction with the Kolmogorov hypothesis for unresolved turbulence to develop a theory to estimate the smallest optically important flow length scale in a general aero-optical framework. According to their analysis, in the limit of high Reynolds numbers, the smallest optically important flow scale does not depend on the Kolmogorov scale. For a given geometry, this length scale depends only on the flow Mach number, free-stream refractive index $n_\infty$, and the optical wavelength $\lambda_0$:

$$\ell_c = C \frac{\lambda_0^{6/7} \ell^{4/7}}{M^{12/7}(n_\infty - 1)^{6/7} z_1^{3/7}}, \tag{13}$$

where $\ell_c$ is the smallest optically active scale, $M$ is the turbulent Mach number, $z_1$ is the depth of the turbulent field in the propagation direction, and $\ell$ is the length scale of the largest turbulent eddy. The proportionality constant $C$ in Equation 13 can be written in terms of the universal constant of the Kolmogorov spectrum and the acceptable energy threshold for the error beam in Equation 12 and is generally of small value; for example, this constant is approximately 0.05 for 95% accuracy (see Mani et al. 2008 for details). A crude estimate based on practical aero-optical parameters indicates that the length scale predicted by this theory is in the inertial range and of the order of typical resolutions for LES in generally accepted practice. This indicates that an adequately resolved LES is sufficient for aero-optical computations without the need for subgrid optical modeling, and DNS is not necessary. Extension of this analysis to complex flow regimes with inhomogeneous turbulence and mesh spacing can be found in Mani et al. (2008).

The results of this analysis and the conclusion regarding negligible optical effects by small-scale turbulence are consistent with the previous experimental findings of Zubair & Catrakis (2007), who verified the "resolution robustness" of optical distortions by systematically examining the refractive-index data of separated shear layers at various resolution levels.

### 4.3. Wave-Front Sensors

The most critical device for experimental aero-optics is the wave-front sensor. The wave front is the locus of constant phase for the complex intensity (see Equation 3). This quantity cannot be measured directly, as any light-recording device is sensitive only to the absolute value of the complex intensity. Wave-front sensors can be divided into several categories depending on how the wave front is measured, which also defines the sensor performance in terms of the dynamic range, temporal and spatial resolution, and sensitivity to real-life corrupting effects such as the quality of the optical elements involved or large jitter of the incoming beam due to mechanical vibration. Interferometry-based sensors combine the measured wave front with a known wave front, which creates an interference pattern with variable light intensity on the sensor, and the measured wave front can be directly reconstructed from it. They have very good spatial (tens of thousands of points) and temporal (up to 100 kHz) resolution but usually require very good optical elements to manipulate the incoming beam before sending it to the sensor. Slope-based sensors, such as a Shack-Hartmann sensor (Tyson 1997), rely on the Huygens' principle, which states that the wave front propagates in the direction normal to itself (Born & Wolf 2002). A lenslet array is used to break the wave front into a large number of small subapertures, and the overall tilt or the deflection angle over each subaperture is measured by tracing the dot motion at the lenslet focal plane. The deflection angles are gradients of the wave front, and different techniques are used to reconstruct the original wave front. These sensors are perhaps the most robust and widely

used wave-front sensors, with a large dynamic range and relative insensitivity to the quality of the optical components and the overall beam jitter. The spatial resolution is, however, limited by the lenselet array, which typically has several thousand subapertures, and temporal resolution is usually limited by the sampling rates of the digital cameras used (up to tens of kilohertz for the most recent cameras). Finally, phase-diversity and distorted-grating sensors use the intensity transport equation to measure the wave front (Blanchard et al. 2000) and ultimately are sensitive to the wave-front curvature. They have good spatial resolution (several thousand points) and very high temporal resolution (up to 100 kHz) but typically require good optical components to manipulate the beam, as well as small overall beam jitter, and selective aperture geometries.

Most wave-front devices use high-speed digital cameras to record images, which contain information about measured wave fronts. For slope-based wave-front sensors, these digital devices limit the sampling speed of data collection. To overcome this problem, researchers developed analog-only wave-front devices, which use photosensitive diodes to record instantaneous deflection angles over subapertures. Examples of these devices include a Malley probe (Gordeyev et al. 2007a), a small-aperture beam technique sensor (Hugo & Jumper 1996), and an analog-only Shack-Hartmann wave-front sensor (Abado et al. 2010). These devices have high sampling rates (~100 kHz) but either measure only a one-dimensional slice of the wave front (the Malley probe) or have limited spatial resolution (small-aperture beam technique sensor, analog-only Shack-Hartmann sensor). As a final note, Equation 13 provides a practical estimate of the minimum number of subapertures needed to correctly measure wave fronts, and for most subsonic flows, only a few thousand subapertures are sufficient for accurate measurements of $\mathrm{OPD}_{rms}$.



## 5. AERO-OPTICAL FLOWS AND DISTORTION MECHANISMS

### 5.1. Turbulent Boundary Layers

The optically aberrating effects of high-speed, turbulent boundary layers have been the subject of research since the early 1950s. The first investigation was by Liepmann (1952) and made use of the jitter angle of a thin beam of light as it traveled through the compressible boundary layer on the sides of high-speed wind tunnels as a way to quantify the crispness on schlieren photographs. Stine & Winovich (1956) performed photometric measurements of the time-averaged radiation field at the focal plane of a receiving telescope, and this work also raised the prospect of using an optical degradation measurement as a method of inferring turbulence scales. Rose (1979) used hot-wire measurements and the linking equation (Equation 8) to estimate aero-optical aberrations caused by turbulent boundary layers and found empirically that $\mathrm{OPD}_{rms} \sim q\delta$, where $q$ is the dynamic pressure and $\delta$ is the boundary-layer thickness. As reviewed by Gilbert & Otten (1982), research up until 1980 focused on the measurement of time-averaged optical distortions, either directly by optically based methods or indirectly using fluid-mechanical measurements and the linking equation.

The development of the high-temporal-resolution Malley probe and other high-speed wave-front devices in recent years allowed accurate time-space-resolved optical measurements in turbulent boundary layers. Wyckham & Smits (2009) investigated the aero-optical performance of transonic and supersonic boundary layers using a two-dimensional Shack-Hartman wave-front sensor. Based on the OPD equation (Equation 5), and by assuming negligible pressure fluctuations in the boundary layer and invoking the strong Reynolds analogy (Morkovin 1962), they proposed the scaling relation $\mathrm{OPD}_{rms} \sim \rho M^2 \delta \sqrt{C_f}\, r_2^{3/2}$, where $C_f$ is the local skin friction coefficient and $r_2$ is the ratio between the bulk and free-stream temperatures ($r_2 \approx 1$ at subsonic speeds). Gordeyev et al. (2011b) employed the linking equation along with the assumption of negligible pressure fluctuations and the strong Reynolds analogy to develop a model for $\mathrm{OPD}_{rms}$ at both

subsonic and supersonic speeds. Their model takes the form $\mathrm{OPD}_{rms} \sim \rho\delta\sqrt{C_f}F_1(M)$, where $F_1(M)$ is a function of the mean and fluctuating velocity profiles and the free-stream Mach number $M$; $F_1(M) \approx M^2$ at subsonic speeds. This model was shown to correctly predict the amplitude and the convective velocity of optically active structures in compressible boundary layers. Both models (Wyckham & Smits 2009, Gordeyev et al. 2011b) were found to generally agree with each other up to $M = 5$.

Nonadiabatic effects with heated and cooled walls were studied by Cress (2010) and Cress et al. (2010). They predicted and experimentally verified that proper cooling of the wall upstream of the aperture will significantly decrease aero-optical distortions. Large intermittent increases of aero-optical aberrations with subsequent dropouts in far-field intensities have also been investigated experimentally (Gordeyev et al. 2003, Cress 2010).

All these experimental studies strongly suggest that the majority of optically active structures in compressible boundary layers are located in the outer region of the boundary layer, moving at 0.82–0.85 times the free-stream velocity. The predominant mechanism for density fluctuations in compressible boundary layers is believed, at least in the time-averaged sense, to be adiabatic heating/cooling due to velocity fluctuations via the strong Reynolds analogy, as pressure fluctuations inside boundary layers are much smaller than temperature fluctuations. This was also confirmed in numerical simulations (Wang & Wang 2011).

Whereas experimental investigations have shed much light on the characteristics and scaling laws of boundary-layer aero-optics, numerical simulations have started to play a significant role in gaining a physical understanding of distortion mechanisms and testing aero-optical theories and their underlying assumptions. High-fidelity approaches such as DNS and well-resolved LES are ideally suited for such fundamental studies because they provide detailed spatial and temporal information about the index-of-refraction field along with the velocity field, making it possible to directly relate flow structures to optical aberrations.

Tromeur et al. (2003, 2006a,b) undertook the first numerical investigation of the optical-aberrating effects of turbulent boundary layers using LES. They considered temporally and spatially evolving flat-plate boundary layers at free-stream Mach numbers of 0.9 and 2.3 and momentum-thickness Reynolds number $Re_\theta = 2{,}917$. Converged flow and optical statistics were obtained and analyzed in the case of spatially developing boundary layers with an adiabatic wall. By comparing directly computed $\mathrm{OPD}_{rms}$ with that obtained using the linking equation (Equation 8) with LES density-fluctuation data, Tromeur et al. (2006a,b) found significant discrepancies between the two and consequently questioned the applicability of the linking equation to boundary-layer flows. However, Wang & Wang (2011) later noted that these discrepancies were caused by the improper choice of the correlation-length definition that is inconsistent with the linking equation.

Wang & Wang (2009, 2011) performed a well-resolved LES study of optical-distortion mechanisms in Mach-0.5, adiabatic-wall boundary layers at $Re_\theta = 875$, 1,770, and 3,550. They obtained detailed statistics of fluctuating-density and wave-front distortions, including the root-mean-square values, spatial and temporal correlations, and frequency spectra. They also evaluated contributions from different boundary-layer regions to wave-front errors, which show dominance of the logarithmic layer and wake region. Consistent with the analysis of Mani et al. (2008), the effect of small-scale flow structures on optical aberrations was found to be small. They re-examined the applicability of Sutton's linking equation, finding that, with a definition of the density correlation length consistent with the linking equation, the latter provides an excellent prediction of $\mathrm{OPD}_{rms}$. The effect of turbulence inhomogeneity is too small to affect the validity of the linking equation. The convection velocities of the optical wave front were computed and found to be consistent with previous experimental values.

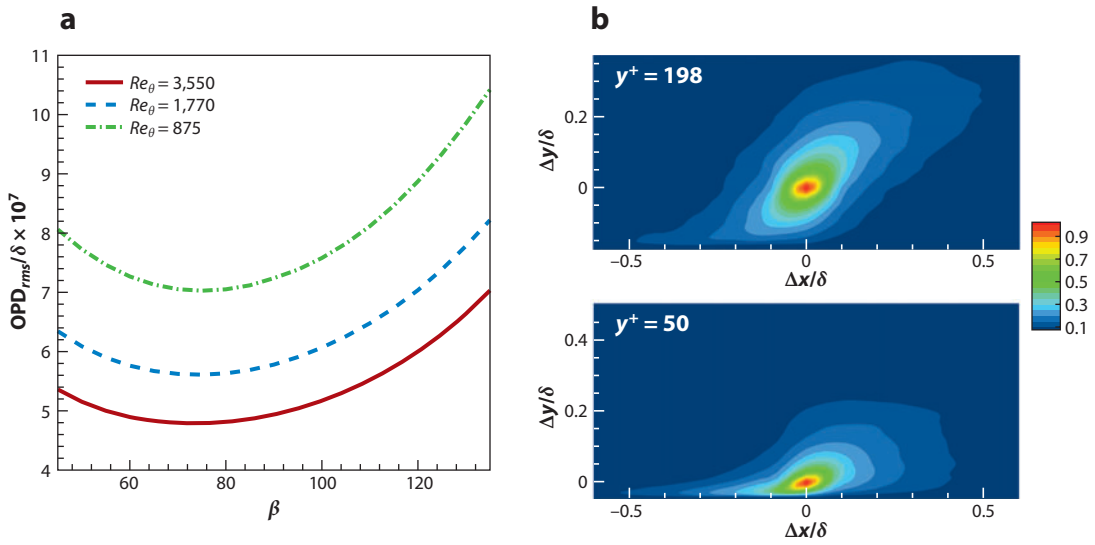


**Figure 3**

(*a*) $OPD_{rms}$ variation with elevation angle (measured from upstream wall) for an optical beam passing through a Mach-0.5 turbulent boundary layer at three different Reynolds numbers. The aperture size is $0.6\delta$ in the streamwise ($x$) and $2.3\delta$ in the spanwise ($z$) direction. (*b*) Two-point spatial correlations of density fluctuations in the $x$-$y$ plane at two wall-normal locations for $Re_\theta = 3{,}550$. The results are obtained from large-eddy simulations (Wang & Wang 2011).

It is well-established that turbulent boundary layers contain packets of vortical structures with a preferred angular direction (e.g., Adrian 2007, Wu & Moin 2009). They are believed to be important sources of aero-optical distortions, and therefore the boundary layer exhibits an anisotropic behavior for different elevation angles of beam propagation. This behavior was measured experimentally (Cress et al. 2008) and later observed computationally (Wang & Wang 2009, 2011). As illustrated in **Figure 3**, a beam is distorted more severely when it is tilted toward the downstream rather than the upstream direction with the same relative angle to the normal direction. This is consistent with the linking-equation prediction (Equation 8) because the correlation length $\Lambda$ is longer when the beam is aligned with the elongated vortical structures in the boundary layer (see **Figure 3*b***). A similar directional dependence of optical distortions was observed by Truman & Lee (1990) in an incompressible DNS of turbulent shear flow with a uniform mean-shear rate.

Although it is generally believed that $OPD_{rms}$ is insensitive to the Reynolds number if the Reynolds number is sufficiently high, the results of Wang & Wang (2011) still exhibit a significant variation of $OPD_{rms}$ with Reynolds number (see **Figure 3**) for fixes boundary-layer thickness and Mach number; however, the rate of variation is seen to decrease with increasing Reynolds number. Simulations at higher Reynolds numbers are required to allow direct, quantitative comparisons with experimental measurements, which are typically performed at much higher Reynolds numbers.

## 5.2. Turbulent Shear Layers and Wakes

Separated turbulent shear layers are omnipresent around aero-optical devices such as turrets and laser cavities. The presence of large-scale vortical structures in shear layers has been firmly established for the past 30 years or so, yet until a few years ago, most models used for aero-optical

aberrations in shear layers largely ignored the role of these structures, assuming that pressure fluctuations inside the shear layer are negligible and using the strong Reynolds analogy to compute density fluctuations. We refer the reader to Fitzgerald & Jumper (2004) for a detailed survey of different shear-layer models.

Vortical structures are characterized by a strong radial pressure gradient accompanied by significant pressure fluctuations. Based on this fact, Fitzgerald & Jumper (2002, 2004) developed a physics-based numerical procedure for approximating the density field, and thus the refractive index, from known two-dimensional velocity-field data for total-temperature-matched shear layers. The velocity, density, and pressure fields are connected by the Euler equations, and by assuming an isentropic process and using a simplified version of the energy equation and the ideal gas law, they developed a procedure for iteratively retrieving density and pressure fields based on the given velocity field. Their model, called the weakly compressible model, takes into account the radial pressure gradients required to sustain the vortical flow and curved path lines. Fitzgerald & Jumper (2004) showed that this model predicted reasonably well the experimentally observed aero-optical aberrations for a high subsonic shear layer, when other shear-layer models failed to do so. However, as a simplified model, its accuracy is limited by its underlying assumptions. A comparison with the numerical results of a compressible shear layer obtained by Visbal (2009) using ILES with a high-order scheme shows that the weakly compressible model, while correctly predicting density fluctuations inside vortical structures, is unable to predict the sharp density gradients numerically observed in braid regions between vortical structures.

To further investigate the nature of this discrepancy, Visbal (2009) performed simulations for laminar mixing layers with either matched total or static temperature of the upper and lower streams. When the total temperature was matched, a density interface between the two streams was apparent in the shear-layer braid regions, although this effect has not been observed experimentally. In contrast, sharp density gradients were absent when the static temperature was matched. Despite the significant differences in the density field, the OPD distributions were similar, indicating that optical distortions are dominated by compressible effects instead of density interfaces.

For transitional mixing layers, Visbal (2009) showed that optical distortions near a splitter plate are similar to those caused by laminar mixing layers and increase downstream as the mixing layer grows. The effects of forcing with either spanwise uniform or nonuniform excitations on turbulent mixing layers have been studied as well (Visbal 2008, White et al. 2010). It was shown that in general, forced mixing layers induce larger OPD, and the forcing regularizes the shear layer, confirming the experimental results of Rennie et al. (2008).

Mani et al. (2009) performed a fundamental study of the optical distortions caused by separated shear layers and wakes using a highly accurate LES with high grid resolution. They considered a Mach-0.4 flow over a circular cylinder at $Re = 3{,}900$ and 10,000. They found that optical distortions by the fully developed wake were insensitive to the Reynolds number, whereas distortions by the separated shear layers were sensitive to it. This finding was explained on the basis that the instability of the wake is predominantly inviscid and that the Reynolds number affects only the Kolmogorov scale, which was found to be optically unimportant (Mani et al. 2008). In contrast, the instability and transition in the early separated shear layers are Reynolds-number sensitive, leading to Reynolds-number sensitivity of their optical effects.

The aero-optics of shear layers with different gases on both sides was studied by Dimotakis et al. (2001), Catrakis & Aguirre (2004), and Zubair & Catrakis (2007), among others. Dimotakis et al. (2001) studied subsonic shear layers at low and high Reynolds numbers with different gases on the two sides. Gases were density matched but had different index-of-refraction coefficients. They took instantaneous snapshots of index-of-refraction fields using the Rayleigh scattering technique and calculated instantaneous wave fronts by integrating the field in the beam-propagation direction.

The large-scale structures in the shear layer were found to be the dominant source for aero-optical distortions, and a level-set model was proposed to explain observed wave-front characteristics. As pointed out by Jumper & Fitzgerald (2001), the combined aero-optical effects were from both index-of-refraction mixing and compressible turbulent mixing, and ultimately, the proposed level-set model underestimated the experimentally measured aero-optical levels of subsonic index-of-refraction-matched compressible shear layers (Fitzgerald & Jumper 2004). Catrakis & Aguirre (2004) also used the Rayleigh scattering technique to study the aero-optical structure in dissimilar-gas mixing layers at high Reynolds numbers. They developed a new interfacial-fluid-thickness approach, based on tracing regions of high gradients of the index-of-refraction field, to study the physics of aero-optical distortions.

## 5.3. Flow over Optical Turrets

Among the most used platforms to point and track lasers are turrets of the hemisphere-on-cylinder type. They provide a convenient way to steer and stay the beam in a desired direction for a transmitting station or to keep a lock on the incoming beam for a receiving station. Most airborne laser-based systems, both past and present, use a form of the turret geometry. But their less-than-ideal aerodynamic shape creates complex flow fields consisting of all major fundamental turbulent flows: boundary layers, separated shear layers, wakes, necklace vortices, and other large-scale vortical structures, as shown schematically in **Figure 4**.

Depending on the viewing direction, the laser beam will encounter one or several of these fundamental flows. Even the time-averaged flow around the turret has significant steady pressure and density gradients, causing steady-lensing effects. Flow is typically attached on the front portion of the turret with a relatively thin boundary layer, so the outgoing laser beam has mostly steady-lensing aberrations imposed on it. Flow is separated on the aft portion of the turret, and when transmitting through the separated region, the beam will experience significant unsteady aero-optical aberrations, even at relatively small subsonic speeds (Gordeyev et al. 2007a,b, 2010b; Vukasinovic et al. 2010). Aero-optical distortions in this region are predominantly caused by shear-layer vortical structures and the separation bubble formed downstream of the turret (see **Figure 4**). At transonic and supersonic flows, shock-induced aero-optical effects with large density gradients are added to this already complicated picture (Gordeyev & Jumper 2010).

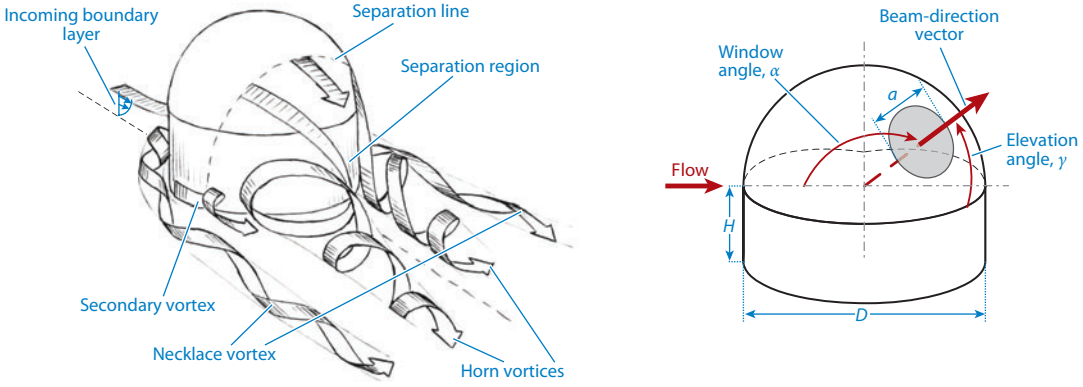


**Figure 4**

Flow topology around an optical turret and measurement coordinates. Figure taken from Gordeyev & Jumper (2010).

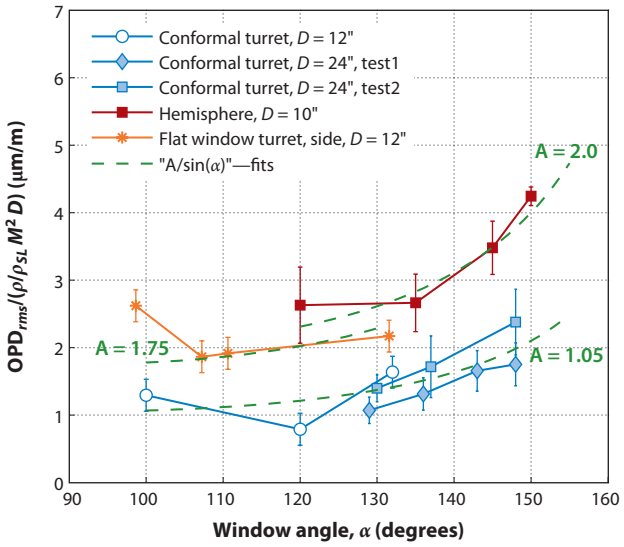


**Figure 5**

Normalized levels of aero-optical distortions induced by turret flows measured for different viewing angles and turret geometries. Figure taken from Gordeyev & Jumper (2010).

Owing to their technological importance, turrets were studied extensively in the 1970s and 1980s, and good reviews of research efforts during that period are provided by Gilbert & Otten (1982) and Sutton (1985). But laser systems of those days had long wavelengths (~10 μm), and unsteady aero-optical effects caused by turrets were found to be negligible at subsonic speeds; only steady-lensing effects were considered. The switch to shorter-wavelength (~1μm) lasers in recent years has exacerbated the aero-optical effects, which spurred a renewed interest in the aero-optics of turrets. A summary of recent efforts, including flow-control strategies to mitigate aero-optical effects around turrets, can be found in Gordeyev & Jumper (2010).

Recent experiments (Gordeyev & Jumper 2010) have shown that for subsonic flows at large Reynolds numbers, $\mathrm{OPD}_{rms} \sim A(\text{geometry}, a/D)B(\alpha, \gamma)\rho_\infty M^2 D$, where $\rho_\infty$ and $M$ are the free-stream density and Mach number, respectively; $D$ is the turret radius; $A$ is a "constant" depending on the turret geometry and the relative aperture size, $a/D$; and $B$ is a function of the beam-transmitting direction, defined by window angle $\alpha$ and elevation angle $\gamma$, shown in **Figure 4**. This simple scaling was found to collapse most of the experimental results available in the open literature (**Figure 5**). The turret geometry was found to influence aero-optical aberrations. A hemispherical turret is more optically aberrating than a hemisphere-on-cylinder turret because of the increased proximity of the near-the-wall vortices to the aperture. A flat-window turret creates more aero-optical distortions compared with a conformal-window turret because of an earlier separation from the front portion of the flat-window aperture.

Numerical simulations of flow over turrets are extremely challenging owing to the complex vortex structures discussed above and the wide range of flow scales associated with them. The high Reynolds numbers encountered at realistic flight or laboratory conditions make these flows out of reach by LES. In addition, simulations must cope with traditional difficulties such as the laminar-to-turbulence transition of the boundary layer and incipient separation from the turret surface. Aside from a few LES attempts (Jones & Bender 2001, Arunajatesan & Sinha 2005), which are grossly under-resolved, most recent computational efforts are based on RANS/LES

hybrid approaches. Nahrstedt et al. (2008) employed the partially averaged Navier-Stokes method (Girimaji & Abdol-Hamid 2005) with the $k - \varepsilon$ model in a finite-volume CFD code to compute the aero-optical flow and $OPD_{rms}$ of a 12-inch-diameter hemispherical/cylindrical turret in a wind-tunnel experiment (Gordeyev et al. 2007b) at Mach numbers ranging from 0.3 to 0.5. With 2.7 million grid points, their results captured some aspects of the experimental measurements, but sizable discrepancies existed, and the vortical structures in the shear and wake were apparently too coherent. Ladd et al. (2009) used DES with the two-equation $k - \omega$ SST model to compute the same flow with a 3.2 million-point structured mesh and a 10 million-cell unstructured mesh and obtained improved solutions. Their mean turret surface pressure and velocity profiles at several wake stations showed reasonable agreement with experimental values, as did their $OPD_{rms}$ over a range of elevation angles. The best-resolved turret-flow simulation to date was performed by Morgan & Visbal (2010), who again considered the experimental configuration of Gordeyev et al. (2007b). Using a hybrid RANS/ILES method with a $k - \varepsilon$ model and a sixth-order compact-difference solver on a 23.6 million-point mesh, their simulation captured fine details of turbulence structures and many flow features observed in the experiment, but there were also significant differences in the separated region. Major discrepancies were observed between the computed $OPD_{rms}$ values and experimental data.

Virtually all numerical simulations of turret flows to date are for turrets with a conformal window. Flows around flat-window turrets are more difficult to study both experimentally and computationally. The slope discontinuity around the flat aperture causes a premature flow separation and creates a weak separation bubble over the aperture at some angles (Gordeyev et al. 2007a, 2010b), leading to increased aero-optical distortions. Aside from increased geometric and flow complexity, computational expenses are higher because a separate flow simulation is required for each viewing angle as the flow field around the turret depends on the window position.

Evidently, current computational capabilities still do not allow accurate and robust predictions of the fluctuating index-of-refraction field around a three-dimensional optical turret at realistic Reynolds numbers. Hybrid LES/RANS methods continue to offer the best practical approach, but a number of weaknesses and outstanding issues need to be addressed. For DES methods, which treat attached boundary layers with RANS, the prediction of boundary-layer transition and incipient separation from the turret surface is a significant challenge. Furthermore, the shear layer immediately after separation, which is in the optically important region, may not behave realistically without upstream turbulence. The effect of upstream turbulent fluctuations on the shear-layer instability and how to incorporate them in DES-type simulations require further investigation.

Given the significant computational challenges for three-dimensional turrets, it would be prudent to first validate solution techniques in simpler flows that capture some crucial physical aspects of realistic turret flows. The two-dimensional cylindrical turret investigated experimentally by Gordeyev et al. (2011a) provides an excellent benchmark configuration for computational validation. Because the turret is mounted horizontally on two flat surfaces of different altitude, the flow upstream of the turret is a flat-plate turbulent boundary layer, which can be easily characterized, and realistic turbulent inflow can be fed into the simulation (Wang & Wang 2009). This configuration has been employed in a number of recent LES investigations (Wang & Wang 2009, Morgan & Visbal 2010, Wang et al. 2010).

## 6. CONCLUDING REMARKS

Aero-optics is an interdisciplinary area that has seen a renewed interest and significant growth over the past decade. At the core of aero-optical phenomena is compressible turbulence, whose

accurate prediction in a practical aero-optical environment over optically active flow scales remains a significant challenge. This review focuses on the fundamental understanding and prediction of aero-optics and related numerical and experimental techniques. Given the diverse nature of the field and space limitations, the contents of this article are necessarily selective; they are by no means reflective of the relative level of research activities or accomplishments. Computational techniques and their applications to aero-optical problems are afforded more coverage considering the growing role of computations and their future promise.

The discussions presented above are mostly on the aero-optical effects of subsonic flows. The presence of shock waves and shock-turbulence interactions in a supersonic flow exacerbates aero-optical effects and gives rise to additional computational and experimental challenges, which are not discussed here. Wave-front sensors and data-reduction algorithms are only briefly mentioned, but they are the most critical part in collecting accurate aero-optical measurements.

Another important aspect of aero-optics research not covered above is mitigation strategies. The goal of aero-optical mitigations is to reduce the overall distortions of an optical beam, which can be achieved through a variety of flow control and/or adaptive-optics techniques. Passive control devices placed in front of an optical turret have shown promise (Gordeyev et al. 2010a), and active flow control using pulsating microjets has effectively reduced aero-optical distortions around turrets (Vukasinovic et al. 2010). Although adaptive optics alone currently works only for low-frequency aberrations typical of atmospheric turbulence, progress has been made in extending it to high-frequency aero-optics. One promising technique, which has been demonstrated in a compressible shear layer (Rennie et al. 2008), involves a combination of adaptive optics with flow control. By first regularizing the flow using active flow control, the aberrations become predictable and can be corrected by a deformable mirror without instantaneous wave-front measurements.

In the development of mitigation techniques for optical systems, a fundamental understanding of aero-optical mechanisms gained through physical and numerical experiments has played and will continue to play an essential role. Further advances in experimental and computational techniques leading to accurate predictive tools are much needed to accelerate the development of practical airborne laser systems.

## DISCLOSURE STATEMENT

The authors are not aware of any biases that might be perceived as affecting the objectivity of this review.

## ACKNOWLEDGMENTS

The authors acknowledge support from the Air Force Office of Scientific Research, the High Energy Laser Joint Technology Office, and the Air Force Research Laboratory for research in this area. We thank Eric Jumper and colleagues in the Aero-Optics Group at the University of Notre Dame and Parviz Moin of Stanford University for many fruitful discussions.

## LITERATURE CITED

Abado S, Gordeyev S, Jumper E. 2010. Two-dimensional high-bandwidth Shack-Hartmann wavefront sensor: design guidelines and evaluation testing. *Opt. Eng.* 49:064403

Adrian RJ. 2007. Hairpin vortex organization in wall turbulence. *Phys. Fluids* 19:041301

Arunajatesan S, Sinha N. 2005. *Analysis of line of sight effects in distortions of laser beams propagating through a turbulent turret flow field.* Presented at AIAA Aerosp. Sci. Meet. Exhib., 43rd, Reno, NV, AIAA Pap. 2005–1081

Blanchard P, Fisher D, Woods SC, Greenaway AH. 2000. Phase-diversity wave-front sensing with a distorted diffraction grating. *Appl. Opt.* 39:6649–55

Born M, Wolf E. 2002. *Principles of Optics*. Cambridge, UK: Cambridge Univ. Press. 952 pp. 7th ed.

Cassady PE, Birch SF, Terry PJ. 1989. Aero-optical analysis of compressible flow over an open cavity. *AIAA J.* 27:758–62

Catrakis HJ, Aguirre RC. 2004. New interfacial fluid thickness approach in aero-optics with applications to compressible turbulence. *AIAA J.* 43:1973–81

Chernov LA. 1960. *Wave Propagation in a Random Medium*. New York: McGraw-Hill. 168 pp.

Childs RE. 1993. *Prediction and control of turbulent aero-optical distortion using large eddy simulation*. Presented at AIAA SDIO Annu. Intercept. Technol. Conf., 2nd, Albuquerque, NM, AIAA Pap. 1993-2670

Coles WA, Filice JP, Frehlich RG, Yadlowsky M. 1995. Simulation of wave propagation in three-dimensional random media. *Appl. Opt.* 34:2089–101

Cress JA. 2010. *Optical aberrations caused by coherent structures in a subsonic, compressible, turbulent boundary layer*. PhD thesis. Univ. Notre Dame

Cress J, Gordeyev S, Jumper E. 2010. *Aero-optical measurements in a heated, subsonic, turbulent boundary layer*. Presented at AIAA Aerosp. Sci. Meet., 48th, Orlando, FL, AIAA Pap. 2010-0434

Cress J, Gordeyev S, Post M, Jumper EJ. 2008. *Aero-optical measurements in a turbulent, subsonic boundary layer at different elevation angles*. Presented at AIAA Plasmadyn. Lasers Conf., 39th, Seattle, AIAA Pap. 2008-4214

Dimotakis PE, Catrakis HJ, Fourguette DC. 2001. Flow structure and optical beam propagation in high–Reynolds number gas-phase shear layer and jets. *J. Fluid Mech.* 433:105–34

Fitzgerald EJ, Jumper EJ. 2002. Scaling aerooptic aberrations produced by high-subsonic-Mach shear layers. *AIAA J.* 40:1373–81

Fitzgerald EJ, Jumper EJ. 2004. The optical distortion mechanism in a nearly incompressible free shear layer. *J. Fluid Mech.* 512:153–89

Frehlich R. 2000. Simulation of laser propagation in a turbulent atmosphere. *Appl. Opt.* 39:393–97

Germano M, Piomelli U, Moin P, Cabot WH. 1991. A dynamic subgrid-scale eddy viscosity model. *Phys. Fluids A* 3:1760–65

Gilbert KG, Otten LJ, eds. 1982. *Aero-Optical Phenomena*. Prog. Astronaut. Aeronaut. Vol. 80. New York: AIAA. 412 pp.

Girimaji SS, Abdol-Hamid KS. 2005 *Partially-averaged Navier-Stokes model for turbulence: implementation and validation*. Presented at AIAA Aerosp. Sci. Meet. Exhib., 43rd, Reno, NV, AIAA Pap. 2005-0502

Goodman JW. 2004. *Introduction to Fourier Optics*. Greenwood Village, CO: Roberts & Co. 466 pp. 3rd ed.

Gordeyev S, Cress JA, Jumper EJ, Cain AB. 2011a. Aero-optical environment around a cylindrical turret with a flat window. *AIAA J.* 49:308–15

Gordeyev S, Cress JA, Smith A, Jumper EJ. 2010a. *Improvement in optical environment over turrets with flat window using passive flow control*. Presented at AIAA Plasmadyn. Lasers Conf., 41st, Chicago, AIAA Pap. 2010-4492

Gordeyev S, Hayden T, Jumper E. 2007a. Aero-optical and flow measurements over a flat-windowed turret. *AIAA J.* 45:347–57

Gordeyev S, Jumper E, Ng T, Cain A. 2003. *Aero-optical characteristics of compressible, subsonic turbulent boundary layer*. Presented at AIAA/ASME/SAE/ASEE Joint Propuls. Conf. Exhib., 41st, Tucson, AZ, AIAA Pap. 2003-3606

Gordeyev S, Jumper E, Vukasinovic B, Glezer A, Kibens V. 2010b. *Hybrid flow control of a turret wake, part II: aero-optical effects*. Presented at AIAA Aerosp. Sci. Meet., 48th, Orlando, FL, AIAA Pap. 2010-0438

Gordeyev S, Jumper EJ. 2010. Fluid dynamics and aero-optics of turrets. *Prog. Aerosp. Sci.* 46:388–400

Gordeyev S, Jumper EJ, Hayden T. 2011b. Aero-optical effects of supersonic boundary layers. *AIAA J.* In press

Gordeyev S, Post M, MacLaughlin J, Ceniceros J, Jumper E. 2007b. Aero-optical environment around a conformal-window turret. *AIAA J.* 45:1514–24

Hardy JW. 1998. *Adaptive Optics for Astronomical Telescopes*. New York: Oxford Univ. Press. 438 pp.

Havener G. 1992. *Optical wave front variance: a study on analytic models in use today*. Presented at AIAA Aerosp. Sci. Meet. Exhib., 30th, Reno, NV, AIAA Pap. 1992-0654

Hugo RJ, Jumper EJ. 1996. Experimental measurement of a time-varying optical path difference by the small-aperture beam technique. *Appl. Opt.* 35:4436–47

Hugo RJ, Jumper EJ. 2000. Applicability of the aero-optic linking equation to a highly coherent, transitional shear layer. *Appl. Opt.* 39:4392–401

Jones MI, Bender EE. 2001. *CFD-based computer simulation of optical turbulence through aircraft flowfields and wakes*. Presented at AIAA Plasmadyn. Lasers Conf., 32nd, Anaheim, CA, AIAA Pap. 2001-2798

Jumper EJ, Fitzgerald EJ. 2001. Recent advances in aero-optics. *Prog. Aerosp. Sci.* 37:299–339

Ladd J, Mani M, Bower W. 2009. *Validation of aerodynamic and optical computations for the unsteady flow field about a hemisphere-on-cylinder turret*. Presented at AIAA Appl. Aerodyn. Conf., 27th, San Antonio, TX, AIAA Pap. 2009-4118

Liepmann HW. 1952. Deflection and diffusion of a light ray passing through a boundary layer. *Tech. Rep. SM-14397*, Douglas Aircr. Co., Santa Monica, CA

Lilly DK. 1992. A proposed modification of the Germano subgrid scale closure method. *Phys. Fluids A* 4:633–35

Lloyd-Hart M. 2003. Taking the twinkle out of starlight. *IEEE Spectr.* 40:22–29

Mahajan VN 1982. Strehl ratio for primary aberrations: some analytical results for circular and annular pupils. *J. Opt. Soc. Am.* 72:1258–66

Mahajan VN. 1983. Strehl ratio for primary aberrations in terms of their aberration variance. *J. Opt. Soc. Am.* 73:860–61

Mani A, Moin P, Wang M. 2009. Computational study of optical distortions by separated shear layers and turbulent wakes. *J. Fluid Mech.* 625:273–98

Mani A, Wang M, Moin P. 2006. Statistical description of free-space propagation of highly aberrated optical beams. *J. Opt. Soc. Am. A* 23:3027–35

Mani A, Wang M, Moin P. 2008. Resolution requirements for aero-optical simulations. *J. Comput. Phys.* 227:9008–20

Maréchal A. 1947. Étude des effets combinés de la diffraction et des aberrations géométriques sur l'image d'un point lumineux. *Rev. Opt. Theor. Instrum.* 26:257–77

Moin P, Mahesh K. 1998. Direct numerical simulation: a tool in turbulence research. *Annu. Rev. Fluid Mech.* 30:539–78

Moin P, Squires KD, Cabot WH, Lee S. 1991. A dynamic subgrid-scale model for compressible turbulence and scalar transport. *Phys. Fluids A* 3:2746–57

Monin AS, Yaglom AM. 1975. *Statistical Fluid Mechanics*. Vol. 2: *Mechanics of Turbulence*. Cambridge, MA: MIT Press. 886 pp.

Morgan PE, Visbal MR. 2010. *Large eddy simulation of flow over a flat-window cylindrical turret with passive flow control*. Presented at AIAA Aerosp. Sci. Meet., 48th, Orlando, FL, AIAA Pap. 2010-0916

Morkovin MV. 1962. Effects of compressibility on turbulent flows. In *Mechanique de la Turbulence*, ed. A Favre, pp. 367–380. Paris: CNRS

Nahrstedt D, Hsia Y-C, Jumper E, Gordeyev S, Ceniceros J, et al. 2008. Wind tunnel validation of computational fluid dynamics–based aero-optics model. *Proc. IMechE* 223(G4):393–406

Piomelli U, Balaras E. 2002. Wall-layer models for large-eddy simulations. *Annu. Rev. Fluid Mech.* 34:349–74

Pond JE, Sutton GW. 2006. Aero-optic performance of an aircraft forward-facing optical turret. *J. Aircr.* 43:600–7

Porter C, Gordeyev S, Zenk M, Jumper E. 2011. *Flight measurements of aero-optical distortions from a flat-windowed turret on the airborne aero-optics laboratory* (*AAOL*). Presented at AIAA Plasmadyn. Lasers Conf., 42nd, Honolulu, AIAA Pap. 2011-3280

Rennie RM, Duffin DA, Jumper EJ. 2008. Characterization and aero-optic correction of a forced two-dimensional weakly compressible shear layer. *AIAA J.* 46:2787–95

Rose WC. 1979. Measurements of aerodynamic parameters affecting optical performance. *Air Force Weapons Lab. Final Rep. AFWL-TR-78-191*, Kirtland Air Force Base, NM

Ross TS. 2009. Limitations and applicability of the Maréchal approximation. *Appl. Opt.* 48:1812–18

Sasiela RJ. 2007. *Electromagnetic Wave Propagation in Turbulence: Evaluation and Application of Mellin Transforms*. Bellingham, WA: SPIE Press. 369 pp. 2nd ed.

Sinha N, Arunajatesan S, Seiner JM, Ukeiley LS. 2004. *Large-eddy simulations of aero-optic flow fields and control application*. Presented at AIAA Plasmadyn. Lasers Conf., 35th, Portland, OR, AIAA Pap. 2004-2448

Smagorinsky J. 1963. General circulation experiments with the primitive equations. I. The basic experiment. *Mon. Weath. Rev.* 91:99–164

Smith RR, Truman CR, Masson BS. 1990. *Prediction of optical phase degradation using a turbulent transport equation for the variance of index-of-refraction fluctuations*. Presented at AIAA Aerosp. Sci. Meet., 28th, Reno, NV, AIAA Pap. 1990-0250

Spalart PR. 2009. Detached-eddy simulation. *Annu. Rev. Fluid Mech.* 41:181–202

Stine HA, Winovich W. 1956. Light diffusion through high-speed turbulent boundary layers. *Res. Memo. A56B21*, NACA, Washington, DC

Steinmetz WJ. 1982. Second moments of optical degradation due to a thin turbulent layer. See Gilbert & Otten 1982, pp. 78–100

Sutton GW. 1969. Effects of turbulent fluctuations in an optically active fluid medium. *AIAA J.* 7:1737–43

Sutton GW. 1985. Aero-optical foundations and applications. *AIAA J.* 23:1525–37

Tatarski VI. 1961. *Wave Propagation in a Turbulent Medium*. New York: McGraw-Hill. 285 pp.

Tromeur E, Garnier E, Sagaut P, Basdevant C. 2003. Large eddy simulations of aero-optical effects in a turbulent boundary layer. *J. Turbul.* 4(5):1–22

Tromeur E, Garnier E, Sagaut P. 2006a. Analysis of the Sutton model for aero-optical properties of compressible boundary layers. *J. Fluids Eng.* 128:239–46

Tromeur E, Garnier E, Sagaut P. 2006b. Large eddy simulation of aero-optical effects in a spatially developing turbulent boundary layer. *J. Turbul.* 7(1):1–28

Truman CR. 1992. *The influence of turbulent structure on optical phase distortion through turbulent shear flows*. Presented at AIAA SDIO Annul Intercept. Technol. Conf., Huntsville, AL, AIAA Pap. 1992-2817

Truman CR, Lee MJ. 1990. Effects of organized turbulence structures on the phase distortion in a coherent optical beam propagating through a turbulent shear flow. *Phys. Fluids A* 2:851–57

Tsai YP, Christiansen WH. 1990. Two-dimensional numerical simulation of shear-layer optics. *AIAA J.* 28:2092–97

Tyson RK. 1997. *Principles of Adaptive Optics*. New York: Academic. 345 pp. 2th ed.

Tyson RK, ed. 2000. *Adaptive Optics Engineering Handbook*. New York: Marcel Dekker. 339 pp.

Visbal MR. 2008. *Effect of flow excitation on aero-optical aberration*. Presented at AIAA Aerosp. Sci. Meet. Exhib., 46th, Reno, NV, AIAA Pap. 2008-1074

Visbal MR. 2009. *Numerical simulation of aero-optical aberration through weakly-compressible shear layers*. Presented at AIAA Fluid Dyn. Conf., 39th, San Antonio, TX, AIAA Pap. 2009-4298

Vukasinovic B, Glezer A, Gordeyev S, Jumper E, Kibens V. 2010. Fluidic control of a turret wake: aerodynamic and aero-optical effects. *AIAA J.* 48:1686–99

Wang M, Moin P. 2002. Dynamic wall modeling for large-eddy simulation of complex turbulent flows. *Phys. Fluids* 14:2043–51

Wang K, Wang M. 2009. *Numerical simulation of aero-optical distortions by a turbulent boundary layer and separated shear layer*. Presented at AIAA Plasmadyn. Lasers Conf., 40th, San Antonio, TX, AIAA Pap. 2009-4223

Wang K, Wang M. 2011. Aero-optical distortions by subsonic turbulent boundary layers. Presented at AIAA Plasmadyn. Lasers Conf., 42nd, Honolulu, AIAA Pap. 2011-3278

Wang K, Wang M, Gordeyev S, Jumper E. 2010. *Computation of aero-optical distortions over a cylindrical turret with passive flow control*. Presented at AIAA Plasmadyn. Lasers Conf., 41st, Chicago, AIAA Pap. 2010-4498

White MD. 2010. High-order parabolic beam approximation for aero-optics. *J. Comput. Phys.* 229:5465–85

White MD, Morgan PE, Visbal MR. 2010. *High-fidelity aero-optical analysis*. Presented at AIAA Aerosp. Sci. Meet., 48th, Orlando, FL, AIAA Pap. 2010-0433

White MD, Visbal MR. 2010. *High-fidelity analysis of aero-optical interaction with compressible boundary layers*. Presented at AIAA Plasmadyn. Lasers Conf, 41st, Chicago, AIAA Pap. 2010-4496

Wolters DJ. 1973. Aerodynamic effects on airborne optical systems. *Tech. Rep. MDC A2582*, McDonnell Douglas Corp., St. Louis, MO

Wyckham CM, Smits AJ. 2009. Aero-optic distortion in transonic and hypersonic turbulent boundary layers. *AIAA J.* 47:2158–68

Wolfe WL, Zizzis GJ. 1978. *The Infrared Handbook*. Arlington, VA: Off. Nav. Res., Dep. Navy

Wu X, Moin P. 2009. Direct numerical simulation of turbulence in a nominally-zero-pressure-gradient flat-plate boundary layer. *J. Fluid Mech.* 630:5–41

Zubair FR, Catrakis HJ. 2007. Aero-optical resolution robustness in turbulent separated shear layers at large Reynolds numbers. *AIAA J.* 45:2721–28